A Luenberger observer design for fault detection and diagnosis of a five-phase PMSG based tidal system

Z. Liu*, **, A. Houari*, M.F. Benkhoris*, M. Machmoum* and T.H. Tang**

*IREENA Laboratory, Université de Nantes
Bd de l'Université, BP 406, 446002, Saint-Nazaire Cedex, France
(e-mail: zhuo.liu@etu.univ-nantes.fr).

** Department of Electrical Automation, Shanghai Maritime University
1550 Haigang Ave, Shanghai, 201306 P.R. China
(e-mail: liuzhuo@stu.shmtu.edu.cn)

Abstract - In generator side, a fault detection and diagnosis (FDD) is proposed based on Luenberger observer with the application to a five-phase tidal current power generation system. A five-phase PMSG dynamic model is firstly presented and then the Luenberger observer-based estimator is designed according to pole placement principles and sensitivity analysis. Thus, this proposed method allows detecting open switch and open phase faults with a rapid fault detecting speed. Simulation validations are presented afterwards respectively under healthy and faulty working conditions. The results show that the designed Luenberger observer owns the high robustness and detectability.

Key words—Fault Detection and Diagnosis, five-phase PMSG, design of a Luenberger observer, sensitivity analysis, tidal system.

1. Introduction

For the purpose of tidal energy extractions, the reliability and availability provide significant preliminaries. Investigation of advanced fault detection and diagnosis (FDD) methods is necessary for this issue, which facilitates the maintenance of power generation system under sea water environments [1-3].

FDD methods can be overall divided into model-based and data-based ones [4]. Here signal-based methods are incorporated into the data-based group due to the demands of data acquisition in practice. This work focuses on the model-based method considering computational burdens and algorithm complexity. Since the data-based methods, especially the artificial intelligence (AI)-based ones, they need collect amount of data for recognition tasks and use some complicated AI methods for FDD. As for model-based ones, the FDD process mainly depends on the residuals, which represents the errors (estimates and measurements) between mathematical model and physical systems. The quantity of residuals is affected by model uncertainties, which can be aroused by disturbances, noises and fault occurrences [5]. In the past several decades, there emerge a great number of successful state estimation methods [6-9], such as Kalman filter, Luenberger observer, sliding mode observer and so forth. The type of Kalman filter methods take accounts of process and measurement noises with a predicting mechanism. However, the optimizing iterations of the time-varying gain need some computations in real-time. Sliding mode observer is able to process the nonlinear problem but with overall complexities of its algorithm. Comparing with the above classical method, Luenberger observer provides a fixed gain of estimating errors

in the initialized stage instead of iterations. In addition, selection of this gain is convenient by using of pole placement approaches concerning the dynamic performance and oscillations. To simplify the process of observer gains' selection, a sensitivity analysis is given in this paper. On the basis of above analysis, a a fault detection and diagnosis (FDD) is proposed based on Luenberger observer is proposed using complete observer design procedures.

2. 1. DYNAMIC MODEL OF FIVE-PHASE PMSG

Fig. 1 indicates synoptic system diagram in generator side of the tidal current generation system. It consists of tidal current, turbine, 5-phase PMSG, generator side converter with five legs, maximum power point tracking (MPPT) unit as well as speed and torque control system.

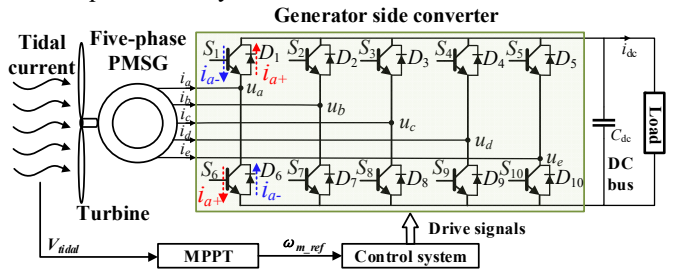


Fig. 1. A tidal current power generation system (generator side)

Assuming that saturation, eddy currents and iron loss are negligible for the 5 phase PMSG. Fig. 2 described the diagram for PMSG windings. Phase shifts of stator mutual inductance M_1 (adjacent phases) and M_2 (non-adjacent phases) are respectively $2\pi/5$ and $4\pi/5$.

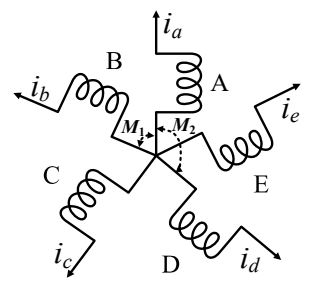


Fig. 2. Five-phase PMSG Stator windings.

Based on the above star-connecting winding, electrical voltage equations of the PMSG in original *abcde* frames written in matrix form is given by

$$\begin{bmatrix} u_{a} \\ u_{b} \\ u_{c} \\ u_{d} \\ u_{e} \end{bmatrix} = \begin{bmatrix} e_{a} \\ e_{b} \\ e_{c} \\ e_{d} \\ e_{e} \end{bmatrix} - R_{s} \begin{bmatrix} i_{a} \\ i_{b} \\ i_{c} \\ i_{d} \\ i_{e} \end{bmatrix} - \begin{bmatrix} L_{s} & M_{1} & M_{2} & M_{2} & M_{1} \\ M_{1} & L_{s} & M_{1} & M_{2} & M_{2} \\ M_{2} & M_{1} & L_{s} & M_{1} & M_{2} \\ M_{2} & M_{2} & M_{1} & L_{s} & M_{1} \\ M_{1} & M_{2} & M_{2} & M_{1} & L_{s} \end{bmatrix} \frac{d}{dt} \begin{bmatrix} i_{a} \\ i_{b} \\ i_{c} \\ i_{d} \\ i_{e} \end{bmatrix}$$

$$(1)$$

where u_i and e_i (i = a, b, c, d, e) respectively represent the phase voltage and the back electromagnetic force (EMF). L_s is the self-inductance of the stator.

$$\begin{bmatrix} u_{\rho\alpha} \\ u_{\rho\beta} \\ u_{s\alpha} \\ u_{o\alpha\beta} \end{bmatrix} = \mathbf{T}_{5} \begin{bmatrix} u_{a} \\ u_{b} \\ u_{c} \\ u_{e} \end{bmatrix} = \sqrt{\frac{2}{5}} \begin{bmatrix} 1 & \cos(\frac{2\pi}{5}) & \cos(\frac{4\pi}{5}) & \cos(\frac{6\pi}{5}) & \cos(\frac{8\pi}{5}) \\ 0 & \sin(\frac{2\pi}{5}) & \sin(\frac{4\pi}{5}) & \sin(\frac{6\pi}{5}) & \sin(\frac{8\pi}{5}) \\ 1 & \cos(\frac{6\pi}{5}) & \cos(\frac{2\pi}{5}) & \cos(\frac{8\pi}{5}) & \cos(\frac{4\pi}{5}) \\ 0 & \sin(\frac{6\pi}{5}) & \sin(\frac{2\pi}{5}) & \sin(\frac{8\pi}{5}) & \sin(\frac{4\pi}{5}) \\ \sqrt{1/2} & \sqrt{1/2} & \sqrt{1/2} & \sqrt{1/2} & \sqrt{1/2} \end{bmatrix} \begin{bmatrix} u_{a} \\ u_{b} \\ u_{c} \\ u_{d} \end{bmatrix}$$

$$(2)$$

5-phase PMSG can be decomposed as primary, secondary and homopolar machines according to $^{[10]}$. In this paper, the EMF of 5-phase PMSG contains two harmonics: the fundamental and the third harmonic associated to the primary and the secondary machine, respectively. Eq. (1) is thus converted to the following equation by applying Concordia transformation T_5 . Furthermore, Park transformation $P(\theta)$ and $P(3\theta)$ are separately applied to the primary machine and the secondary machine. The rotation transformation is presented as Eq. (3).

$$\begin{bmatrix}
 [u_{pd} \\ u_{pq}] = \mathbf{P}(\theta) \begin{bmatrix} u_{p\alpha} \\ u_{p\beta} \end{bmatrix} = \begin{bmatrix} \cos(\theta) & \sin(\theta) \\ -\sin(\theta) & \cos(\theta) \end{bmatrix} \begin{bmatrix} u_{p\alpha} \\ u_{p\beta} \end{bmatrix} \\
 [u_{sd} \\ u_{sq}] = \mathbf{P}(3\theta) \begin{bmatrix} u_{s\alpha} \\ u_{s\beta} \end{bmatrix} = \begin{bmatrix} \cos(3\theta) & \sin(3\theta) \\ -\sin(3\theta) & \cos(3\theta) \end{bmatrix} \begin{bmatrix} u_{s\alpha} \\ u_{s\beta} \end{bmatrix}$$
(3)

Finally, the electrical voltage equation for 5-phase PMSG in *dq*0 frames is eventually deduced as Eq. (4).

$$\begin{cases} u_{pd} = e_{pd} - R_s i_{pd} - L_{pr} \frac{di_{pd}}{dt} + \omega_e L_{pr} i_{pq} \\ u_{pq} = e_{pq} - R_s i_{pq} - L_{pr} \frac{di_{pq}}{dt} - \omega_e L_{pr} i_{pd} \end{cases}$$

$$\begin{cases} u_{sd} = e_{sd} - R_s i_{sd} - L_{se} \frac{di_{sd}}{dt} + 3\omega_e L_{se} i_{sq} \\ u_{sq} = e_{sq} - R_s i_{sq} - L_{se} \frac{di_{sq}}{dt} - 3\omega_e L_{se} i_{sd} \end{cases}$$

$$\begin{cases} u_{odq} = e_{odq} - R_s i_{odq} - L_{odq} \frac{di_{odq}}{dt} (homopolar machine) \end{cases}$$

$$\begin{cases} u_{odq} = e_{odq} - R_s i_{odq} - L_{odq} \frac{di_{odq}}{dt} (homopolar machine) \end{cases}$$

here $L_{pr}=L_s+\frac{\sqrt{5}-1}{2}M_1-\frac{\sqrt{5}+1}{2}M_2$, $L_{se}=L_s-\frac{\sqrt{5}+1}{2}M_1+\frac{\sqrt{5}-1}{2}M_2$ and $L_{0dq}=L_s+2M_1+2M_2$ are the equivalent inductance for primary, secondary and homopolar machines. e_{pd} , e_{pq} , e_{sd} , e_{sq} and e_{0dq} are the electromotive force under dq0 frames. Their expressions are given by

$$e_{0dq} = e_{pd} = e_{sd} = 0, e_{pq} = \sqrt{\frac{5}{2}} \cdot \omega_e \Phi_1, e_{sq} = \sqrt{\frac{5}{2}} \cdot 3\omega_e \Phi_3$$
 (5)

where Φ_1 and Φ_3 are respectively the permanent magnet flux from the first and third harmonics.

3. Luenberger Observer-Based FDD Method

Based on the model of applications described in section 2, the main principle of a design for Luenberger observer-based FDD method is presented in this part.

3.1. Luenberger observer by five-phase PMSG model

First of all, according to Eq. (4) and Eq. (5), the matrix form of five-phase PMSG model is given in Eq. (6). The general state space model is thus expressed as

$$\begin{cases} \dot{x}(t) = \mathbf{A}x(t) + \mathbf{B}u(t) + \mathbf{De}(t) \\ y(t) = \mathbf{C}x(t) \end{cases}$$
 (7)

where C = (1,1,1,1) by neglecting the component of homopolar machine. observability is determined by matrix $[C, CA, CA^2, CA^3]^T$, which means there exists a unique output during a finite period for every initial condition. In this paper, the system is observable with a full rank. Therefore, the Luenberger state-observer expression is thus given by

$$\hat{\mathbf{x}}(t) = \mathbf{A}\hat{\mathbf{x}}(t) + \mathbf{B}u(t) + \mathbf{D}\mathbf{e}(t) + \mathbf{L}\mathbf{u}(y(t) - \hat{y}(t))$$

$$\hat{\mathbf{y}}(t) = \mathbf{C}\hat{\mathbf{x}}(t)$$
(8)

where state correction matrix $\mathbf{Lu}(y(t) - \hat{y}(t))$ illustrates the relationship between measured and estimated terms and \mathbf{Lu} is a 4×4 matrix as Eq. (9). The 2×2 square matrix in the upper left corner \mathbf{Lu}_{pr} and lower right corner \mathbf{Lu}_{se} are respectively the gain matrix for primary machine and secondary machine.

$$\mathbf{L}\mathbf{u} = \begin{bmatrix} \mathbf{L}\mathbf{u}_{pr} & 0\\ 0 & \mathbf{L}\mathbf{u}_{se} \end{bmatrix} = \begin{bmatrix} Lu_{pr1} & Lu_{pr3} & 0 & 0\\ \frac{Lu_{pr4}}{0} & \frac{Lu_{pr2}}{0} & 0 & \frac{0}{Lu_{se1}} & \frac{Lu_{se3}}{Lu_{se3}}\\ 0 & 0 & Lu & Lu_{se3} \end{bmatrix}$$
(9)

The above gain reflects the dynamic vibrations of the Luenberger observer. With Eq. (7) and Eq. (8), the complete expression of Luenberger observer is given by

$$\dot{x}(t) = \left[\mathbf{A} - \mathbf{L}\mathbf{u}\mathbf{C}\right]\hat{x}(t) + \mathbf{B}u(t) + \mathbf{D}\mathbf{e}(t) + \mathbf{L}\mathbf{u}y(t)$$
 (10)

where u is the input of the observer, y is the output of original model in Eq. (7). **De** can be treated as the disturbances owing to fluxes of machine.

$$\begin{bmatrix}
\frac{di_{pd}}{dt} \\
\frac{di_{pq}}{dt} \\
\frac{di_{sd}}{dt} \\
\frac{di_{sq}}{dt} \\
\frac{di_{sq}}{dt} \\
\frac{di_{odq}}{dt}
\end{bmatrix} = \begin{bmatrix}
-\frac{R_s}{L_{pr}} & \omega_e & 0 & 0 & 0 \\
-\omega_e & -\frac{R_s}{L_{pr}} & 0 & 0 & 0 \\
0 & 0 & -\frac{R_s}{L_{se}} & 3\omega_e & 0 \\
0 & 0 & -3\omega_e & -\frac{R_s}{L_{se}} & 0 \\
0 & 0 & 0 & 0 & -\frac{R_s}{L_{odq}}
\end{bmatrix} \begin{bmatrix}
i_{pd} \\
i_{pd} \\
i_{sq} \\
i_{odq} \\
i_{odq}
\end{bmatrix} - \begin{bmatrix}
1 \\
L_{pr} & 0 & 0 & 0 & 0 \\
0 & \frac{1}{L_{pr}} & 0 & 0 & 0 \\
0 & 0 & \frac{1}{L_{se}} & 0 & 0 \\
0 & 0 & 0 & \frac{1}{L_{odq}}
\end{bmatrix} \begin{bmatrix}
u_{pd} \\
u_{pq} \\
u_{sd} \\
u_{qq} \\
u_{0dq}
\end{bmatrix} + \begin{bmatrix}
5 \\
5 \\
2 \\
2 \\
2 \\
2 \\
2 \\
0
\end{bmatrix}$$

$$(6)$$

3.2. FDD method based on designed Luenberger observer

Main design for a Luenberger observer is given in section 3.1 and 3.2. After these preparations, here a current form factor is introduced for the needs of FDD. The overall diagram of the FDD method is shown in Fig. 4.

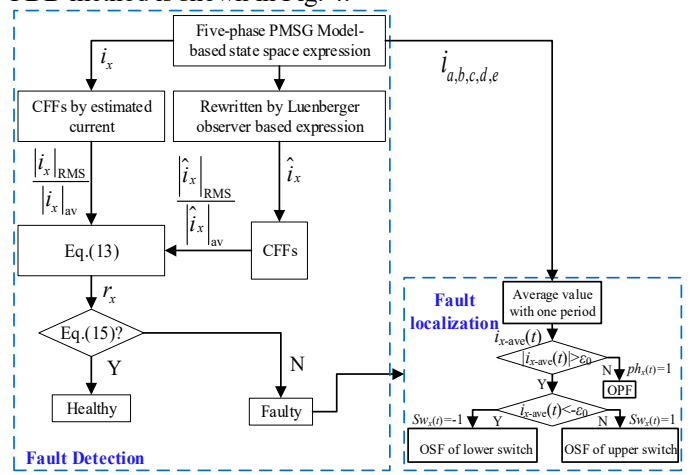


Fig. 3. Diagram of Luenberger based FDD method.

To obtain current form factors (CFFs), measured current and estimated current are given by

$$i_{cff_{-}x}(t) = \frac{|i_{x}(t)|_{RMS}}{|i_{x}(t)|_{av}}, \hat{i}_{cff_{-}x} = \frac{|\hat{i}_{x}(t)|_{RMS}}{|\hat{i}_{x}(t)|_{av}} \text{ where } x=a,b,c,d,e$$
 (11)

The RMS value reflects the variation of distance for phase currents from their corresponding average values, and is sensitive by deviations from the unrectified average values, such as in faulty conditions. Thus, here CFFs are utilized for fault detections.

For each phase, a residual is generated and expressed as

$$r_x(t) = \hat{i}_{cff_x}(t) - i_{cff_x}(t)$$
 (12)

Then the adaptive threshold is build up with the following equation:

$$r_{x}(t) = \frac{\left|i_{x}(t) + e_{x}(t)\right|_{\text{RMS}}}{\left|i_{x}(t) + e_{x}(t)\right|_{\text{av}}} - \frac{\left|i_{x}(t)\right|_{\text{RMS}}}{\left|i_{x}(t)\right|_{\text{av}}}$$
(13)

where e_x is the observer error given by

$$e_{x}(t) = \hat{i}_{x}(t) - i_{x}(t)$$
 (14)

Then the above residuals can be organized as:

$$r_{x}(t) \leq \frac{\left|i_{x}(t)\right|_{\text{RMS}}}{\left|i_{x}(t) + e_{x}(t)\right|_{\text{av}}} + \frac{\left|e_{x}(t)\right|_{\text{RMS}}}{\left|i_{x}(t) + e_{x}(t)\right|_{\text{av}}} - \frac{\left|i_{x}(t)\right|_{\text{RMS}}}{\left|i_{x}(t)\right|_{\text{av}}}$$
(15)

Finally, the adaptive threshold can be expressed by

$$Th_{x}(t) = \eta \frac{\left| e_{x}(t) \right|_{\text{RMS}}}{\left| i_{x}(t) \right|_{\text{av}}}$$
(16)

where η is the gain coefficient to tune appropriate thresholds in practice to enhance efficiency of fault detection.

After that, average current values i_{x_av} are selected associated with faulty legs to achieve accurate fault localizations. In addition, a threshold Th_0 is defined for fault localizations.

$$i_{x_{-}av}(t) = \frac{1}{T(t)} \int_{t-T(t)}^{T(t)} (i_{x}(t)) dt$$
 (17)

3.3. Selecting gain of Luenberger observer

Gain of Luenberger observer has an effect on the estimating errors, which directly influence the performance of FDD. Here a pole placement method is thus given. Illustrations of detectability are carried out by sensitivity analysis.

3.3.1. Performance analysis by pole placement

The observer error is supposed to be calculated by the eigenvalues of (**A-LuC**) and placed at the left half *s*-plane. Importantly, these eigenvalues should meet the demands of fast response and accurate current estimation for the five-phase PMSG power conversion system. The calculation is derived by the subspace of primary machine and secondary machine as

$$\begin{cases} \det(s\mathbf{I} - (\mathbf{A}_{pr} - \mathbf{L}\mathbf{u}_{pr}\mathbf{C}_{pr})) = (s - \lambda_{pr1})(s - \lambda_{pr2}) = 0 \\ \det(s\mathbf{I} - (\mathbf{A}_{co} - \mathbf{L}\mathbf{u}_{co}\mathbf{C}_{co})) = (s - \lambda_{co1})(s - \lambda_{co2}) = 0 \end{cases}$$
(18)

Eq. (18) can be thus solved into Eq. (19). The observer eigenvalues can be figured out by Eq. (20).

A standard form of second order characteristic equation and its eigenvalues are given by

$$\begin{cases} s^2 + 2\zeta\omega_n + \omega_n^2 = 0\\ \lambda_{s1,s2} = -\zeta\omega_n \pm j\omega_n \sqrt{1 - \zeta^2} = \sigma + j\omega_d \end{cases}$$
 (21)

where ω_n , ω_d , ζ and σ are respectively undamped natural frequency, damped natural frequency, damping ratio and decay rate. Further in Fig. 3, the geometric relationships of them can be plotted in a complex *s*-plane by their eigenvalues. Here ω_n

$$\begin{cases} \det \left[s + \frac{R_s}{L_{pr}} + Lu_{pr1} - \omega_e + Lu_{pr3} \right] \\ -\omega_e + Lu_{pr4} - s + \frac{R_s}{L_{pr}} + Lu_{pr2} \right] = s^2 + f_{pr} \left(Lu_{pr1}, Lu_{pr2} \right) s + g_{pr} \left(Lu_{pr1}, Lu_{pr2}, Lu_{pr3}, Lu_{pr4} \right) \end{cases} \\ = s^2 + \left(\frac{2R_s}{L_{pr}} + Lu_{pr1} + Lu_{pr2} \right) s + \left(\frac{R_s}{L_{pr}} + Lu_{pr1} \right) \left(\frac{R_s}{L_{pr}} + Lu_{pr2} \right) + \left(\omega_e - Lu_{pr3} \right) \left(\omega_e + Lu_{pr4} \right) \end{cases}$$

$$\det \left[s + \frac{R_s}{L_{se}} + Lu_{se1} - 3\omega_e + Lu_{se3} \right] \\ = s^2 + f_{se} \left(Lu_{se1}, Lu_{se2} \right) s + g_{se} \left(Lu_{se1}, Lu_{se2}, Lu_{se3}, Lu_{se4} \right) \right] \\ = s^2 + \left(\frac{2R_s}{L_{se}} + Lu_{se1} + Lu_{se2} \right) s + \left(\frac{R_s}{L_{se}} + Lu_{se1} \right) \left(\frac{R_s}{L_{se}} + Lu_{se2} \right) + \left(3\omega_e - Lu_{se3} \right) \left(3\omega_e + Lu_{se4} \right) \right] \\ = s^2 + \left(\frac{2R_s}{L_{se}} + Lu_{se1} + Lu_{se2} \right) s + \left(\frac{R_s}{L_{se}} + Lu_{se2} \right) + \left(3\omega_e - Lu_{se3} \right) \left(3\omega_e + Lu_{se4} \right) \\ \left(\lambda_{s-pr1,s-pr2} = \frac{-f \left(Lu_{pr1}, Lu_{pr2} \right)}{2} \pm \frac{j}{2} \sqrt{f \left(Lu_{pr1}, Lu_{pr2} \right)^2 - 4g \left(Lu_{pr1}, Lu_{pr2}, Lu_{pr3}, Lu_{pr4} \right)} \\ \lambda_{s-pr1,s-pr2} = \frac{-f \left(Lu_{se1}, Lu_{se2} \right)}{2} \pm \frac{j}{2} \sqrt{f \left(Lu_{se1}, Lu_{se2} \right)^2 - 4g \left(Lu_{se1}, Lu_{se2}, Lu_{se3}, Lu_{se4} \right)} \end{cases}$$

$$(20)$$

represents the distance from the origin to complex conjugate roots. According to the principles of root locus analysis, the real parts of the eigenvalues of Eq. (20) decides the converging speed of Luenberger observer errors. That is, greater negative real parts of the eigenvalues contribute higher stability and faster dynamic response. Conversely, system will perform worse stability and slower dynamic response when the eigenvalues are close to imaginary axis. However, a too large negative real parts of the eigenvalues results in more sensitive to the noises and even breaks the stability of system.

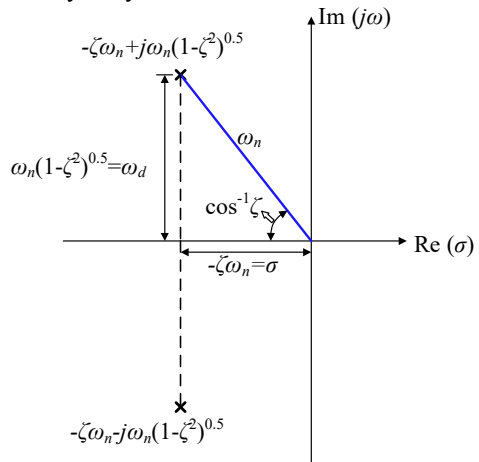


Fig. 4. Diagram of eigenvalues in a complex s-plane

The dynamic performance of observers in Eq. (8) is related to the real parts of the eigenvalues, which is more concerned to obtain fast fault detecting performance in transient states instead of the stability issues. And the dynamic response is related to the eigenvalues while they are affected by the gains Lu_{pr1} , Lu_{pr2} , Lu_{se1} and Lu_{se2} . Here denotes P_{pr1} , P_{pr2} and P_{se1} , P_{se2} are respectively the poles of the system. In addition, to improve dynamic performance of the observer, the eigenvalues of Luenberger observer should be a little more negative than the dominant system poles. Placement of observer poles is limited by considering the inferences noise and dominant system poles.

3.3.2. Sensitivity anaylsis

As a result, a sensitivity analysis should be done to evaluate the detectability of the residuals as faults or uncertainties (e.g. noises) are introduced. Considering the effects by fault signal f and noise δ , here two sensitivity ratios are defined as

$$\begin{cases}
SR_{fx} = \begin{cases}
\frac{r_x(t)}{Th_x} \times 100\%, \ e(t) \ge 0 \\
\frac{r_x(t)}{-Th_x} \times 100\%, \ e(t) < 0
\end{cases}
, SR_{fx} \in [1, +\infty)$$

$$SR_{nx} = \frac{\delta(t)}{Th_x} \times 100\%, SR_{nx} \in [0, 1)$$

As the above expressions, SR_{fx} is supposed to be as large as possible when tuning Luenberger observer gain **Lu** to fit the observer for healthy and faulty conditions. Conversely, SR_{nx} should be as low as possible for the thinking of anti-noise interference. That is, magtitude of noises are much lower than Th_f when the poles in Eq. (20) move towards negative infinity. Notice that noise signal conforms a Gaussian distribution as $\delta(t) \sim N(0, R_c)$ and normalized as residuals, where R_c is the variation of $\delta(t)$. Obviously, SR_{fx} and SR_{nx} will respectively reduce and increase as the observer gain **Lu** increases. The problem of determining various observer gain **Lu** is transformed into trading off between SR_{fx} and SR_{nx} within their boundaries.

4. SIMULATION ANALYSIS

Considering tidal current profiles process a feature of long period over time. In a short period (e.g. one day), the tidal current velocity can be regarded as a constant value. Hence, simulation validations are carried out under a constant rated tidal speed and SNR=60dB. By using MATLAB/SIMULINK, the overall simulation platform is depicted in Fig. 5. In addition, Table 1 lists the main parameters of the platform.

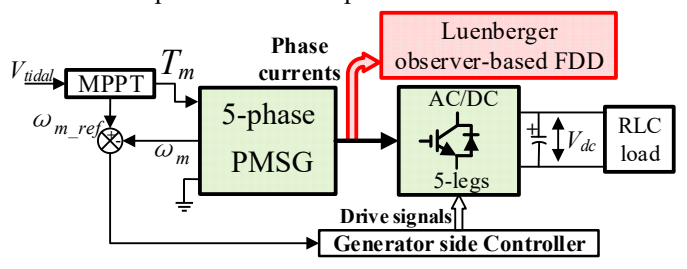


Fig. 5. Brief simulation block diagram.

Table 1. Main parameters of the simulation platform

Symbol	Description	Value
P_m	Generator rated power	1.5 MW
V_{dc}	DC-bus rated voltage	1700 V
n_{pp}	Number of pole pairs	120
Φ_1, Φ_3	Primary and secondary machines' magnet flux	2.458, 0.082 Wb
R_s	Stator resistance	0.0081 Ω
L_{pr}, L_{se}	Primary and secondary machines' inductances	0.4, 0.088mH
f_{pwm}	PWM switching frequency	5kHz
Lu	Gain of Luenberger observer	5×10 ⁵
ω_{s}	SOGI' resonant frequency	5kHz
th_0	Boundary of null zone	0.01
th_f	Threshold for fault detection	7×10 ⁷

4.1. Fault detection and diagnosis performance

Open phase fault and open switch fault will be discussed in this part respectively. Open switch fault (OSF) at the switch S_1 , S_6 and open phase fault (OPF) in phase 'a' are respectively in Fig. 6 to Fig. 8. For all the presented cases, input mechanical torque varies from rated torque to 2/3 rated torque at 0.04s and the faults occur at 0.07s for OSF and 0.06s for OPF. For phase current $i_a(t)$, observer error r_a will be exceed the threshold Tf_a when fault occurs. It can be observed that the fault indications from CFFs residuals r_x are the same from Fig. 6 and Fig. 8, which means no distinguishing capability by the CFFs residuals but great robustness of torque variations. Therefore, average phase current is accordingly used to complete the task of fault identifications. Overall, fault can be effectively detected for OSF and OPF within around 0.0035s.

4.2. Dynamic performance

According to Eq. (8), (13) and (16), the only different part with estimated and observed components is the iterative errors. Larger gains of observer (Lu_{pr1} , Lu_{pr2} , Lu_{se1} and Lu_{se2}) will produce faster dynamic response in dynamic transient states. And the estimated current will be thus more close to the measured current. The threshold will decrease accordingly for fault detection, which makes the system more vulnerable to the occurrence of fault alarms. Therefore, the tradeoff of anti-

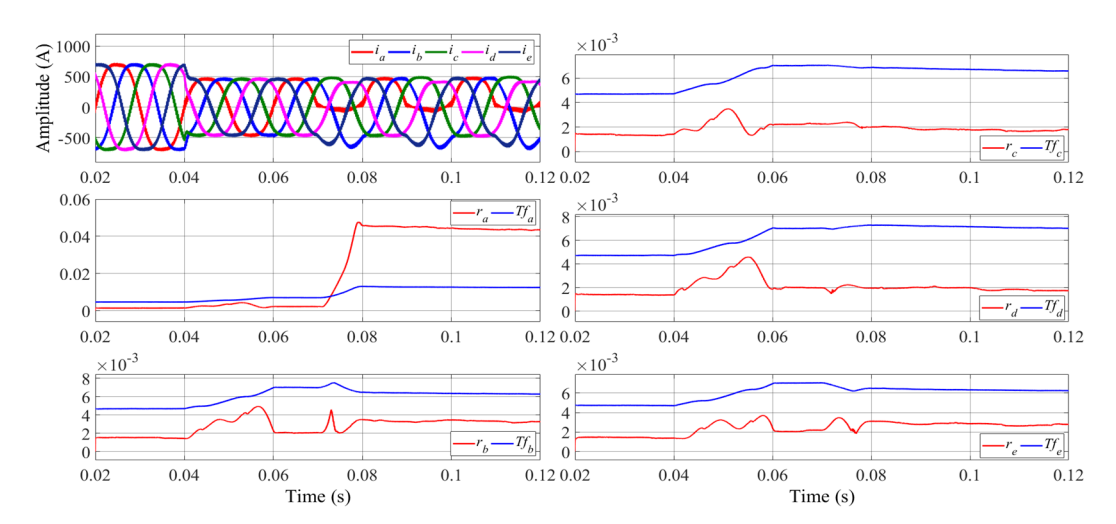


Fig. 6. Open switch fault (S_1 is open at 0.07s)

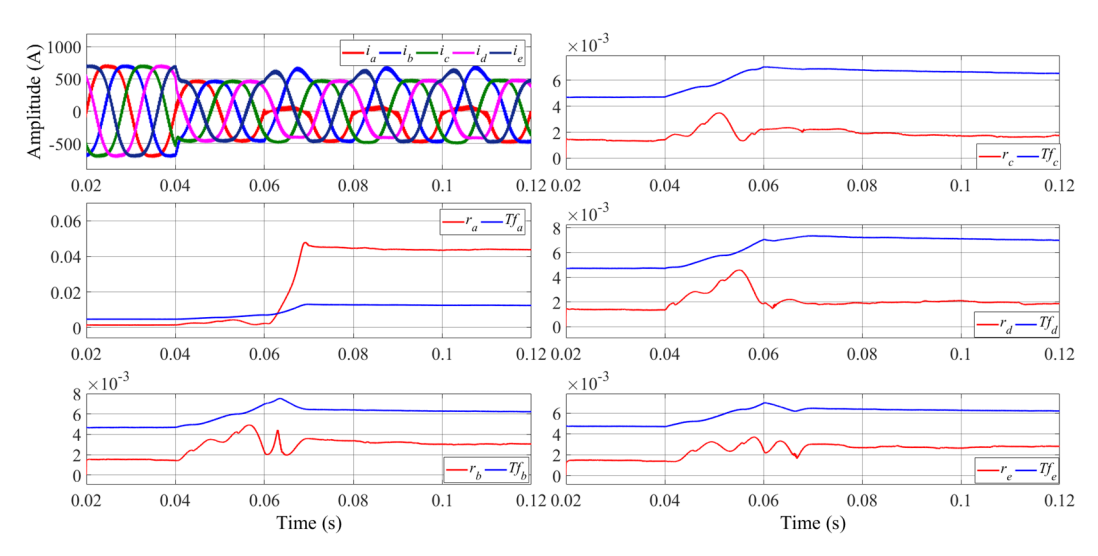


Fig. 7. Open switch fault (S₆ is open at 0.06s)

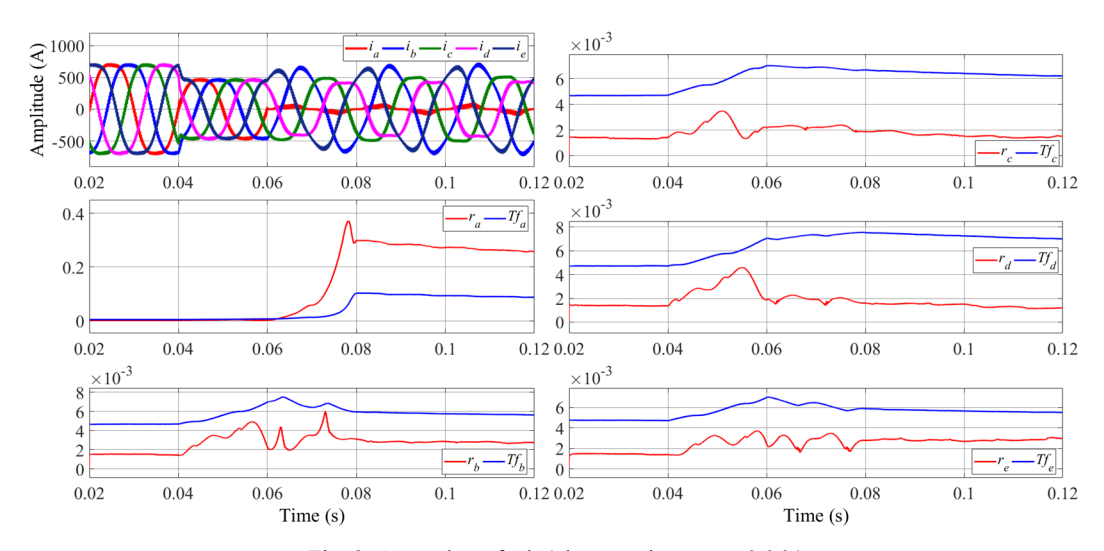


Fig. 8. Open phase fault (phase 'a' is open at 0.06s)

interference ability and dynamic response should be determined depending on the practical demands. For example, the following figure presents the threshold will decrease as gains of observer become higher. Theoretically, lower threshold will lead to higher chances of fault alarms. For ease of comparisons, here Lu_{pr1} , Lu_{pr2} , Lu_{se1} and Lu_{se2} are set as same values.

As the illustrations from 0.04s to 0.06s in Fig. 10 (a) that S_6 is open at 0.065s, average level of the sensitivity ratios in Eq. (23)

during a continuous-time varying process are thus respectively presented in Fig. 10 (b) and (c). With the increasing of observer gains from 5e3 to 1e5, the detectability and estimation accuracy are improved but more vulnerable to noises. Additionally, noises will become dominant components with larger gains. Therefore, the observer gain should be limited with a certain range. In this paper, observer gains are set as 50000 after synthesizing above concerns.

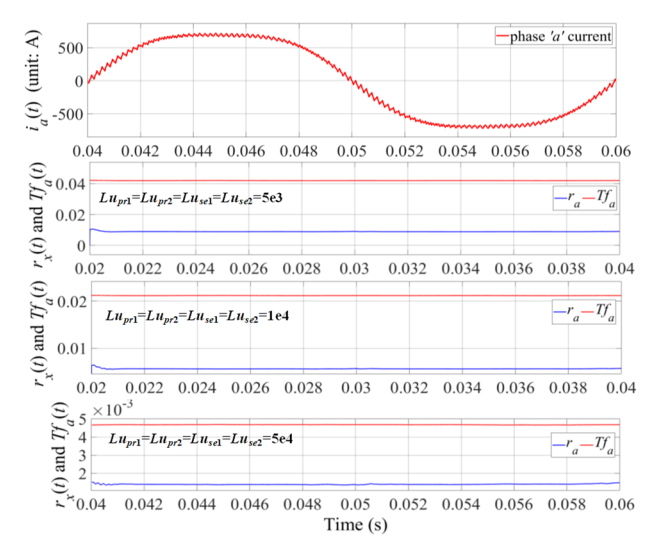
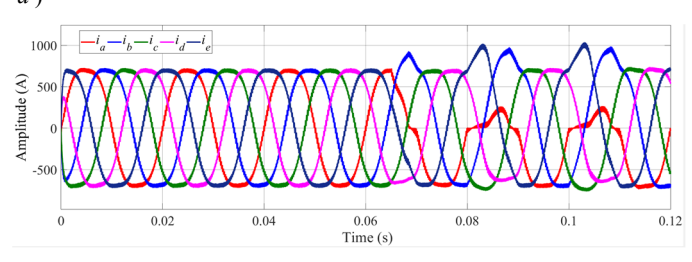
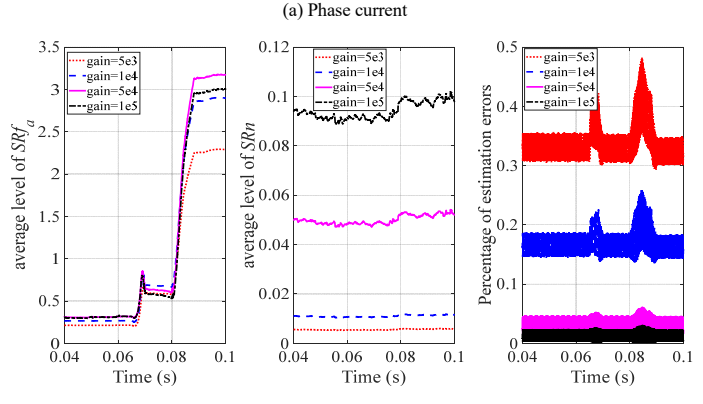


Fig. 9. Detectable variables with various observer gains (e.g. in phase 'a')





(a) Sensitivity ratio of faults (b) Sensitivity ratio for noises (c) estimation accuracy

Fig. 10. Detectability test in healthy and faulty conditions

By relative positions of observer poles and dominant system poles, observer poles will definitely have a left shift by using the feedback gain **Lu**. Therefore, selection of gain **Lu** is supposed to concern synthetization of sensitivity ratios.

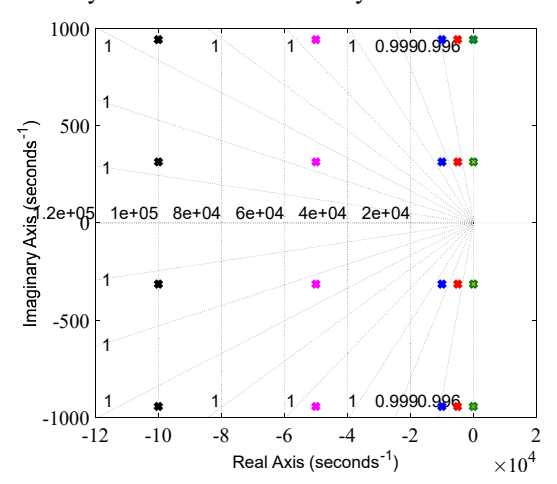


Fig. 11. Pole-zero map of the observer system with various gains

5. CONCLUSIONS

This paper focuses on a model-based FDD issue by a proposed Luenberger observer-based fault estimation method and its application to a tidal current energy system. This FDD scheme beneficiates to a processing procedure of estimating residuals incorporating current form factors. Fault localization is achieved by average phase current. Poles placement and sensitivity analysis allow to facilitate selections of proper observer gains of Luenberger observer in order to increase detectability and robustness of this method. Simulation results show that the FDD scheme works efficiently with satisfied robustness in continuous time process. In the future, the design of the observer is supposed to be implemented under variable tidal speed working conditions.

6. ACKNOWLEDGMENT

This work is finished in IREENA laboratory. This project is supported by China Scholarship Council (NO. 201808310083) and the projects of NSFC (NO. 61673260).

7. References

- [1] Titah-Benbouzid, H and Benbouzid, M. 2015, "Marine renewable energy converters and biofouling: a review on impacts and prevention," In Proceedings of the 11th Europen Wave and Tidal Energy Conference (EWTEC 2015), Nantes, France, 2015, pp. 6-11
- [2] M. Hulse, J. Cronin and M. Tupper, "Advanced Composite Materials for Tidal Turbine Blades, "Materials Challenges in Alternative and Renewable Energy, Ceramic Transactions, Volume 224. 2011.
- [3] W. Zhang, G. Fu, D. Feng, et al, "Decision framework for feasibility analysis of introducing the steam turbine unit to recover industrial waste heat based on economic and environmental assessments", Journal of Cleaner Production, vol. 137, pp.1491-1502, 2016.
- [4] Isermann, R.: 'Combustion engine diagnosis Biology' (Springer Vieweg, 2017), pp. 295-297.
- [5] B. T. Thumati and S. Jagannathan, "A Model-Based Fault-Detection and Prediction Scheme for Nonlinear Multivariable Discrete-Time Systems With Asymptotic Stability Guarantees," in IEEE Transactions on Neural Networks, vol. 21, no. 3, pp. 404-423, March 2010.
- [6] H. Soliman, I. Soliman, E. Mahmoud, and A. K. Ayman. "Post-Fault Speed Sensor-Less Operation Based on Kalman Filter for a Six-Phase Induction Motor", International Journal of Engineering Research. Volume 04, Issue 02; February – 2018.
- [7] G. H. B. Foo, X. Zhang and D. M. Vilathgamuwa, "A Sensor Fault Detection and Isolation Method in Interior Permanent-Magnet Synchronous Motor Drives Based on an Extended Kalman Filter," in IEEE Transactions on Industrial Electronics, vol. 60, no. 8, pp. 3485-3495, Aug. 2013.
- [8] I. Jlassi, J. O. Estima, S. K. El Khil, N. M. Bellaaj and A. J. M. Cardoso, "A Robust Observer-Based Method for IGBTs and Current Sensors Fault Diagnosis in Voltage-Source Inverters of PMSM Drives," in IEEE Transactions on Industry Applications, vol. 53, no. 3, pp. 2894-2905, May-June 2017.
- [9] M. Salehifar, R. Salehi Arashloo, M. Moreno-Eguilaz, V. Sala and L. Romeral, "Observer-based open transistor fault diagnosis and fault-tolerant control of five-phase permanent magnet motor drive for application in electric vehicles," in IET Power Electronics, vol. 8, no. 1, pp. 76-87, 2015.
- [10] I. González-Prieto, M. J. Duran, N. Rios-Garcia, F. Barrero and C. Martín, "Open-Switch Fault Detection in Five-Phase Induction Motor Drives Using Model Predictive Control," in IEEE Transactions on Industrial Electronics, vol. 65, no. 4, pp. 3045-3055, April 2018.